

Viewing-angle expansion of holographic image using enhanced-NA Fresnel hologram

Byung Gyu Chae

Holographic Contents Research Laboratory,

Electronics and Telecommunications Research Institute,

218 Gajeong-ro, Yuseong-gu, Daejeon 34129, Republic of Korea

Abstract

This study presents the theoretical foundation for optimizing the enhanced-NA Fresnel hologram to recover the low space-bandwidth. Optical kernel functions in real and Fourier spaces act as a basis function in digital hologram synthesis. The higher spectrum components of the optical kernel functions beyond the bandwidth exists in the form of their replications. The expansion of angular spectrum of the digital hologram by its repetition during optimization procedure increases the image resolution, resulting in a viewing angle that is dependent on the hologram numerical aperture. We numerically and experimentally verify our strategy to implement a wide viewing-angle holographic display without shrinking the image size.

I. INTRODUCTION

A holographic display is an optical imaging system that forms a three-dimensional image in free space [1]. The spatial resolution of a focused image is explained by the Abbe diffraction limit [2–5], where the lateral resolution represented as the hologram numerical aperture (hNA) has a direct connection with the angular field view of the holographic image. When the hologram is recorded, the geometric structure, which is the ratio of the hologram aperture size to the distance, specifies the range of viewing angle Ω [6]:

$$\Omega = 2 \sin^{-1}(\text{hNA}). \quad (1)$$

The hNA is given by the maximum spatial frequency f_{\max} of the hologram fringe, $\text{hNA} = \lambda f_{\max}$, where λ is the wavelength of the recoding wave. In an analog hologram, this value can determine the viewing angle because nanoscale recording materials are usable. In a holographic display, the digital hologram is encoded on a pixelated spatial light modulator (SLM) with a finite pixel pitch. To realize a holographic image with a wide viewing-angle, the wavelength-scale SLM should be developed. Several researchers have tried to tackle this problem by expanding the diffraction zone in terms of spatial and temporal multiplexing of the pixelated modulator [7–9], or the use of the spatial grid with a fine pitch [10, 11].

In the strategy to expand the diffraction zone, it is natural for the upper bound of viewing angle to exist in a specific pixelated modulator. However, it is not simple because of the sampling characteristics of the digital hologram. When the sampling rate is larger than the bandwidth of the digital hologram, aliased errors occur according to the Nyquist sampling criterion [12–14]. This type of alias error is non-trivial unlike simple aliasing in conventional image processing. We previously reported that in numerical and optical experiments [14, 15], the aliasing effect creates replica fringes of the original pattern, contributing to the reconstruction of the original image with a high resolution. That is, the replica fringes still play a role as components of the higher angular spectrum producing a propagating diffraction field into a wide angular region. This phenomenon is caused by the unusual properties of an optical kernel function with a quadratic phase. We defined this type of digital hologram implying non-trivial aliasing errors as the enhanced-NA Fresnel hologram [14].

This type of Fresnel hologram reconstructs the holographic image within a finite image space to evade the interference of high-order terms. High-order images result from the deviation of the sampling conditions in the hologram plane. Thus, to reconstruct a holographic

image at a wide angle while maintaining the image size, an algorithm for removing the aliasing errors should be developed.

In this letter, we present the algorithm that adequately synthesize an enhanced-NA Fresnel hologram to recover its low bandwidth. A crucial idea exists in using the replication properties of optical kernel functions in real and Fourier spaces. First, we describe the theoretical basis of the proposed algorithm and examine the characteristics of the synthesized digital hologram and the reconstructed image. Further, numerical and optical experiments are performed to confirm the proposed concept for accomplishing viewing-angle expansion without sacrificing the image space.

II. THEORETICAL ANALYSIS FOR THE EXPANSION OF ANGULAR SPECTRUM

The sampling condition of the digital hologram can be interpreted from the calculated diffraction field in digitized space. The Fresnel field $g(x, y)$ propagating between an object $o(x', y')$ and a hologram plane is obtained using the following equation [1]:

$$g(x, y) = \frac{e^{ikz}}{i\lambda z} \exp \left[\frac{i\pi}{\lambda z} (x^2 + y^2) \right] \mathbf{FT} \left[o(x', y') \exp \left[\frac{i\pi}{\lambda z} (x'^2 + y'^2) \right] \right], \quad (2)$$

where k is the wavenumber of $2\pi/\lambda$, z is the propagation distance, and \mathbf{FT} is the Fourier transform. The enhanced-NA Fresnel hologram is synthesized at a distance shorter than the critical distance z_c , as illustrated in Fig. 1(a). The critical distance, $z_c = N\Delta x^2/\lambda$ is defined by the sampling conditions in both planes, $\Delta x = \frac{\lambda z}{N\Delta x'}$ [14, 16]. We adopted a one-dimensional description for the sampling analysis, where Δx and $\Delta x'$ indicate the pixel pitches in the respective planes consisting of $N \times N$ pixels. The lateral resolution of the object image is finer than the hologram pixel pitch. We previously studied the dependency of the viewing angle of the reconstructed image on the hologram numerical aperture [6],

$$\text{hNA} = \sin \left(\frac{\Omega}{2} \right) = \frac{N\Delta x}{2z}, \quad (3)$$

which determines the image resolution. Here, the viewing angle is larger than the diffraction angle by a hologram pixel pitch, $\theta = 2 \sin^{-1} \left(\frac{\lambda}{2\Delta x} \right)$. This value increases at a shorter distance because of the large hNA, in Fig. 1(b). This type of hologram suffers from aliased errors owing to undersampling, but the original image can be completely retrieved. The Fresnel

matrix undersampled by a regular interval still has a unitary property, which enables stable recovery under a severe aliasing error [14].

However, the image space is confined to the diffraction zone by a hologram pixel to avoid the interference of high-order diffractions, as shown in Fig. 1. Algorithms consisting of the double Fourier transform are effective method for calculating the digital hologram using the object space beyond the diffraction scope. In this algorithm, the hologram pixel pitch is calculated via the pixel quantity Δf of the intermediate Fourier plane, $\Delta x = \frac{1}{N\Delta f} = \Delta x'$, and thus, the sizes of the hologram and object are the same:

$$g(x, y) = \mathbf{IFT} \left(\mathbf{FT} [o(x', y')] \mathbf{FT} \left[\exp \left[\frac{i\pi}{\lambda z} (x'^2 + y'^2) \right] \right] \right). \quad (4)$$

On the other hand, the high-frequency components of digital hologram are ruled out because only the zeroth-order region in the intermediate Fourier plane, $N\Delta f$ is used, in Fig. 2(a).

In the enhanced-NA Fresnel hologram, the high-frequency components are recorded as aliased replica fringes, as depicted in Fig. 1(a). The aliased fringes are patterns undersampled by a hologram pixel pitch larger than the required value in the sampling condition. The Fourier-transformed data does not include a higher angular spectrum of the hologram field. This characteristic fundamentally prohibits aliased errors in both planes, as reported in a previous research [6]. By cropping the aliasing fringes, hNA is maintained at a constant value irrespective of the distance, that is, the viewing angle does not vary.

To overcome this limitation, a higher angular spectrum should be utilized during the algorithm process. Optical kernel functions in real and Fourier spaces play a role as a basis function in digital hologram synthesis. We investigated the properties of the optical kernel functions when being sampled, that is, the impulse response function in the real space,

$$h(x, y) = \frac{e^{ikz}}{i\lambda z} \exp \left[\frac{i\pi}{\lambda z} (x^2 + y^2) \right] \quad (5)$$

and the transfer function in the frequency domain,

$$H(f_x, f_y) = e^{ikz} \exp \left[-i\pi\lambda z (f_x^2 + f_y^2) \right]. \quad (6)$$

The response function is the convolutional kernel used to calculate the hologram field, where this function itself becomes a complex hologram for a point object $\delta(x, y)$. Likewise, the transfer function is the angular spectrum of the point's hologram. Digital hologram of an object with a finite size is characterized by the summation of individual functions.

The Fourier transform of sampled response function by a regular interval Δx is given by

$$\mathbf{FT} \left[\sum_n h(n\Delta x) \delta(x - n\Delta x) \right] = \frac{1}{\Delta x} \sum_p H \left(f - \frac{p}{\Delta x} \right). \quad (7)$$

Taking the inverse Fourier transform into the right term of Eq. (7), we get the modulated form of this function, which is rewritable in the shifted form of continuous quadratic functions [15, 17],

$$\sum_n h(n\Delta x) \delta(x - n\Delta x) = \frac{1}{\Delta x} \sum_n c_n h \left(x + \frac{\lambda z n}{\Delta x} \right). \quad (8)$$

The replica functions are formed at a reduced period of $\lambda z/(s\Delta x)$ when the function is undersampled by s multiples of Δx . We find that the high angular spectrum of hologram field is recorded in the form of replica fringes. This type of alias error is non-trivial, unlike the simple aliasing phenomenon in a conventional image. Similarly, when the transfer function is sampled, the same form as that in Eq. (8) is obtained:

$$\sum_q H(q\Delta f) \delta(f - q\Delta f) = \frac{1}{\Delta f} \sum_q c_q H \left(f + \frac{q}{\lambda z \Delta f} \right). \quad (9)$$

The higher angular spectra could also be recorded into their aliased replica fringes. The cropped high-frequency components of the digital hologram in Fig. 2(a) can be restored by expanding the bandlimited transfer function in the angular spectrum space, where its expansion process is carried out from its replication during optimization procedure, as depicted in Fig. 2(b). Finally, the above properties of the optical kernel functions lead to the revival of the high-frequency components in the enhanced-NA Fresnel hologram. Furthermore, the higher order terms in Eq. (8) can be directly reinterpreted as high-order diffractions in the wave-based propagation model. The high-order diffractions act as the high-frequency components of the diffracted wave, indicating that in a digitized imaging system, the resolution performance would be enhanced only if the high-order diffractions are used.

III. EXPERIMENTAL RESULTS AND DISCUSSIONS

We developed the optimization algorithm to expand the angular spectrum of enhanced-NA Fresnel hologram, which is based on gradient descent method, as depicted in Fig. 3. The gradient descent optimization has been known to show a great performance in hologram synthesis such as neural holography [18, 19]. The complex-valued hologram g at respective iteration is updated by minimizing the loss function J , i.e. the squared error between the

original image and reconstructed image, $g_{i+1} = g_i + \alpha \Delta J$. The calculation is performed by the inverse operation of Eq. (4), where to revive the high frequency components, the angular spectrum G of the digital hologram was expanded via its repetition process of m multiples. The corresponding transfer function was also extended to m -multiple frequency space, and the sinc function by a pixelated structure was multiplied. Finally, the reproduced image undergoing m -fold increase in spatial resolution was downsampled to match the original resolution. There was no averaging process for pixels because the high-resolution property of the reconstructed image should be conserved.

Figures 4 shows the simulation results obtained based on the proposed scheme. An object image consisting of 512×512 pixels with an $8\text{-}\mu\text{m}$ pixel pitch and the plane wave with a wavelength of 532 nm were used. The critical distance z_c for this specification is computed to be 61.6 mm. The directly calculated Fresnel hologram using the “HOLOGRAM” letter image at a distance of half of z_c shows that the aliased replica fringes are cropped in the vertical direction because of the use of only the zeroth-order region in the angular spectrum space, as illustrated in Fig. 4(a). The lateral size of the active area in the hologram is two times smaller than the original size. The value decreases in proportion to the located distance of the object image. Based on Eq. (3), hNA is constant irrespective of the distance, thus preventing the increase of the viewing angle. The viewing angle Ω of the reconstructed image has the same quantity as the diffraction angle θ of 3.8° .

Figure 4(b) is the digital hologram synthesized by using the proposed algorithm. The angular spectrum was expanded to 3 multiples in the intermediate process. The aliased fringes in the angular spectrum appear in the seamless form among the replicas after optimization, in Fig. 4(c). We find that the active region of the hologram field occupies the entire area of the digital hologram, which was clearly confirmed on a logarithmic scale. The digital hologram made at a distance of half z_c undergoes two-fold increase in hNA. Further, we confirmed this expansion of the hologram field in the synthesized hologram at a distance of quarter z_c . Figures 4(d) is the reconstructed image in this algorithm, which becomes a standard for algorithm performance. Here, the simulated phase hologram was used. The high-order images in the vertical direction are not completely removed. On the other hand, the dense image occupying the entire area of the object space is well reconstructed without obstructing high-order images, as shown in Figs. 4(e) and 4(f). The PSNR values of the reproduced images from the holograms placed at half- z_c and quarter- z_c distances are esti-

mated to be approximately 30.9 dB and 27.1 dB, respectively. The angular spectrum of a digital hologram made at a quarter- z_c distance was extended to a 5-multiple scope to cover sufficient high-frequency components.

Figure 5 illustrates the diffractive waves that propagate away from the focused images. The phase hologram is taken from the complex modulation because it accelerates convergence in the algorithm, even when using a severely sparse object. Measuring the spreading angle of the diffractive wave is robust method for confirming the viewing angle [20]. The Fresnel transform with a single Fourier transform based on Eq. (2) was used to exclude an artificial expansion of the angular spectrum because it confines an angular view. The intensity of a particular vertical line in the letter image is displayed with a propagating distance. We can observe that the spreading angle increases with decreasing synthesis distance of the digital hologram, indicating that the viewing angle is larger at a shorter synthesis distance. The viewing angle of the reconstructed image from the digital hologram made at a critical distance is estimated to be about 3.7° . The reconstructed images at half- z_c and quarter- z_c distances reveal viewing angles of approximately 7.0° and 13.1° , respectively. It can be confirmed that the proposed algorithm restores the images at a viewing angle dependent on hNA.

Optical experiments were carried out by using a phase-only SLM (Holoeye PLUTO) with 1920×1080 pixels of an $8\text{-}\mu\text{m}$ pixel pitch and a green laser with a wavelength of 532 nm. A digital hologram of 1024×1024 pixels was prepared, in which the zero values were filled outside the bounds. The hologram made at half- z_c , 61.6 mm reconstructs the original letter image without the interference of the high-order noises, as displayed in Fig. 6(a). The polarization filtering technique was used to eliminate the non-diffracted beams. Noise remnants exist in the vertical direction due to the vacant space. When the view of the direction angularly moves the first-order viewing zone, the zeroth-order image is still viewable, in Fig. 6(b). Therefore, the viewing angle is twice as large as the diffraction angle. However, the first-order image appears, and overlaps with the zeroth-order image.

The high-order noises in the viewing zone should be removed to realize a holographic display. In the proposed algorithm, high-order terms are generated from the expansion of the angular spectrum, but it would have a limitation to the removal of high-order diffraction waves because only the reconstructed image in the plane vertical to the central axis is used during the repetition process [20, 21]. When the conjugated waves corresponding to

high-order diffractions are created from the hologram, high-order noises will be completely compensated. Recently, it was reported that the optical filter can block high-order diffractive beams [22]. Figure 6(c) shows the captured image through the optical filter (532 nm MaxLine laser clean-up filter, Semrock). The first-order image in Fig. 6(b) is clearly suppressed by blocking its carrier beam. The high-frequency components emanating in close proximity of the hologram are not affected by an angular spatial filter placed away from the hologram. It has a difficulty in expanding the viewing angle using the synthesized hologram at a quarter- z_c unlike the simulation results. This is considered to be due to the limitation of algorithm such as downsampling of reconstructed image. The development of the advanced optimization algorithm as like learning-based technology would recover these weaknesses.

IV. CONCLUSIONS

We present a method in which a digital hologram with a finite bandwidth generates a holographic image at a viewing angle higher than the diffraction angle, where the image space is not confined to the diffraction zone. The expansion of the angular spectrum in Fourier space leads to the viewing angle dependent on the numerical aperture of the digital hologram. The proposed algorithm is limited to removing high-order diffractive waves, which is eliminated by using an appropriate optical filter. This technique expanding the viewing angle enables us to commercialize the holographic display even using the conventional spatial light modulator.

This work was partially supported by Institute for Information & Communications Technology Promotion (IITP) grant funded by the Korea government (MSIP) (2017-0-00049)

-
- [1] J. W. Goodman, *Introduction to Fourier Optics* (McGraw-Hill, 1996).
 - [2] P. Picart and J. Leval, "General theoretical formulation of image formation in digital Fresnel holography," *J. Opt. Soc. Am. A* **25**(7), 1744-1761 (2008).
 - [3] D. P. Kelly, B. M. Hennelly, N. Pandey, T. J. Naughton, and W. T. Rhodes, "Resolution limits in practical digital holographic systems," *Opt. Eng.* **48**(9), 95801 (2009).
 - [4] T. Latychevskaia and H.-W. Fink, "Inverted Gabor holography principle for tailoring arbitrary shaped three-dimensional beams," *Sci. Rep.* **6**, 26312 (2016).

- [5] M. Kanka, R. Riesenberger, and H. J. Kreuzer, “Reconstruction of high-resolution holographic microscopic images,” *Opt. Lett.* **34**(8), 1162-1164 (2009).
- [6] B. G. Chae, “Analysis on angular field of view of holographic image dependent on hologram numerical aperture in holographic display,” *Opt. Eng.* **59**(3), 035103 (2020).
- [7] T. Kozacki, M. Kujawińska, G. Finke, B. Hennelly, and N. Pandey, “Extended viewing angle holographic display system with tilted SLMs in a circular configuration,” *Appl. Opt.* **51**(11), 1771-1780 (2012).
- [8] K. Yamamoto, Y. Ichihashi, T. Senoh, R. Oi, and T. Kurita, “3D objects enlargement technique using an optical system and multiple SLMs for electronic holography,” *Opt. Express* **20**(19), 21137-21144 (2012).
- [9] Y. Takaki and S. Uchida, “Table screen 360-degree three-dimensional display using a small array of high-speed projectors,” *Opt. Express* **20**(8), 8848-8861 (2012).
- [10] E. Buckley, A. Cable, N. Lawrence, and T. Wilkinson, “Viewing angle enhancement for two- and three-dimensional holographic displays with random superresolution phase masks,” *Appl. Opt.* **45**(28), 7334-7341 (2006).
- [11] J. Park, K. Lee, and Y. Park, “Ultrathin wide-angle large-area digital 3D holographic display using a non-periodic photon sieve,” *Nat. Commun.* **10**, 1304 (2019).
- [12] L. Onural, “Sampling of the diffraction field,” *Appl. Opt.* **39**(32), 5929-5935 (2000).
- [13] A. Stern and B. Javidi, “Analysis of practical sampling and reconstruction from Fresnel fields,” *Opt. Eng.* **43**(1), 239-250 (2004).
- [14] B. G. Chae, “Analysis on image recovery for on-axis digital Fresnel hologram with aliased fringe generated from self-similarity of point spread function,” *Opt. Commun.* **466**, 125609 (2020).
- [15] B. G. Chae, “Wide viewing-angle holographic display based on enhanced-NA Fresnel hologram,” *Opt. Express* **29**(23), 38221-38236 (2021).
- [16] D. Mas, J. Garcia, C. Ferreira, L. M. Bernardo, and F. Marinho, “Fast algorithms for free-space diffraction patterns calculations,” *Opt. Commun.* **164**, 233-245 (1999).
- [17] L. Onural, “Some mathematical properties of the uniformly sampled quadratic phase function and associated issues in Fresnel diffraction simulations,” *Opt. Eng.* **43**(11), 2557-2563 (2004).
- [18] Y. Peng, S. Choi, N. Padmanaban, and G. Wetzstein, “Neural holography with camera-in-the-loop training,” *ACM Trans. Graph.* **39**(6), 185:1-185:14 (2020).

- [19] S. Choi, M. Gopakumar, Y. Peng, J. Kim and G. Wetzstein, “Neural 3D holography: Learning accurate wave propagation models for 3D holographic virtual and augmented reality displays,” *ACM Trans. Graph.* **40**(6), 240:1-240:12 (2021).
- [20] B. G. Chae, “Expansion of image space in enhanced-NA Fresnel holographic display,” *Appl. Sci.* **12**, 4148 (2022).
- [21] M. Gopakumar, J. Kim, S. Choi, Y. Peng, and G. Wetzstein, “Unfiltered holography: optimizing high diffraction orders without optical filtering for compact holographic displays,” *Opt. Lett.* **46**(23), 5822-5825 (2021).
- [22] K. Bang, C. Jang, and B. Lee, “Compact noise-filtering volume gratings for holographic display,” *Opt. Lett.* **44**(9), 2133-2136 (2019)

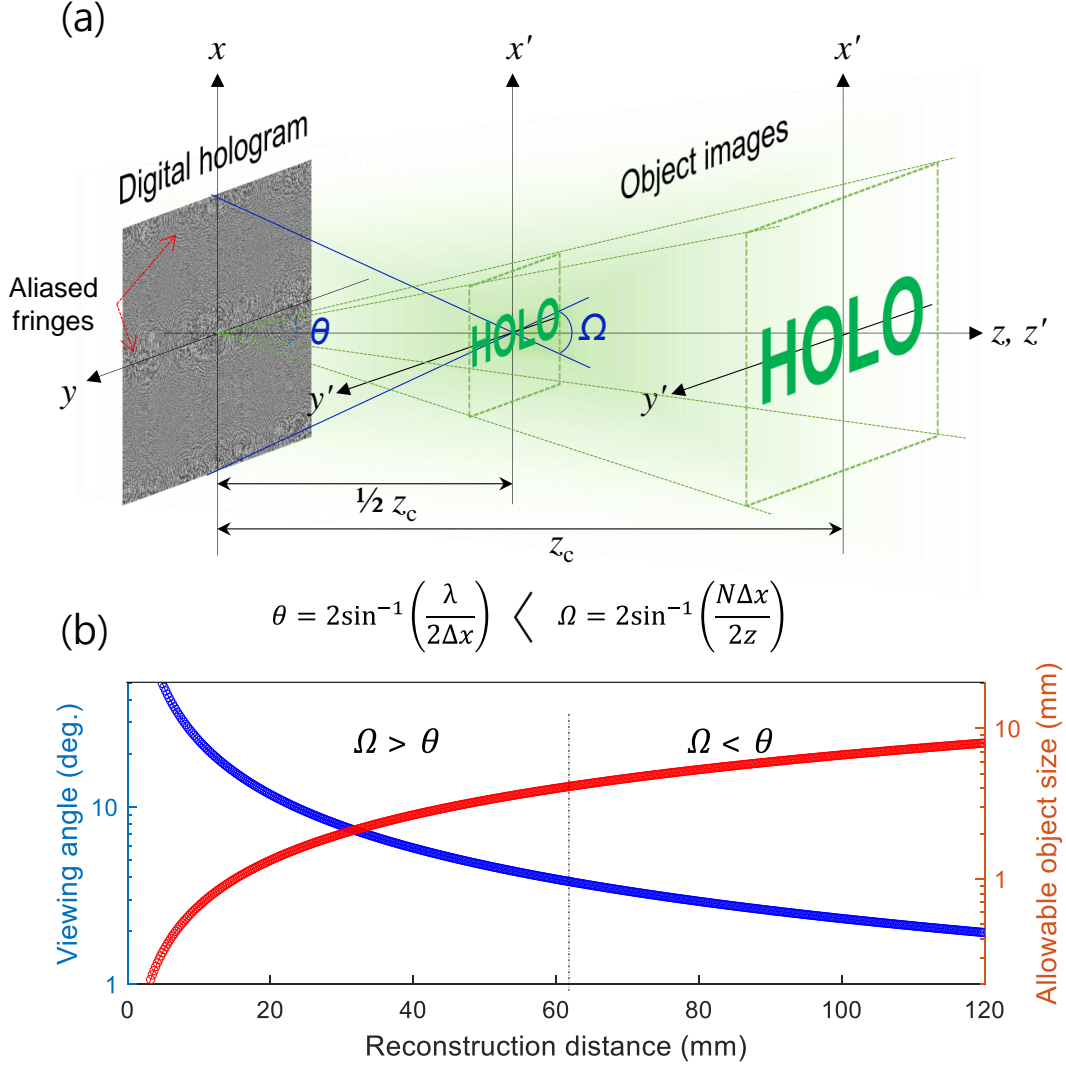


FIG. 1: Schematic of the enhanced-NA Fresnel holographic display system. (b) Changes in the viewing angle and allowable object size with a reconstruction distance. Diffraction angle for digital hologram consisting of 512×512 pixels with an $8\text{-}\mu\text{m}$ pixel pitch is 3.8° .

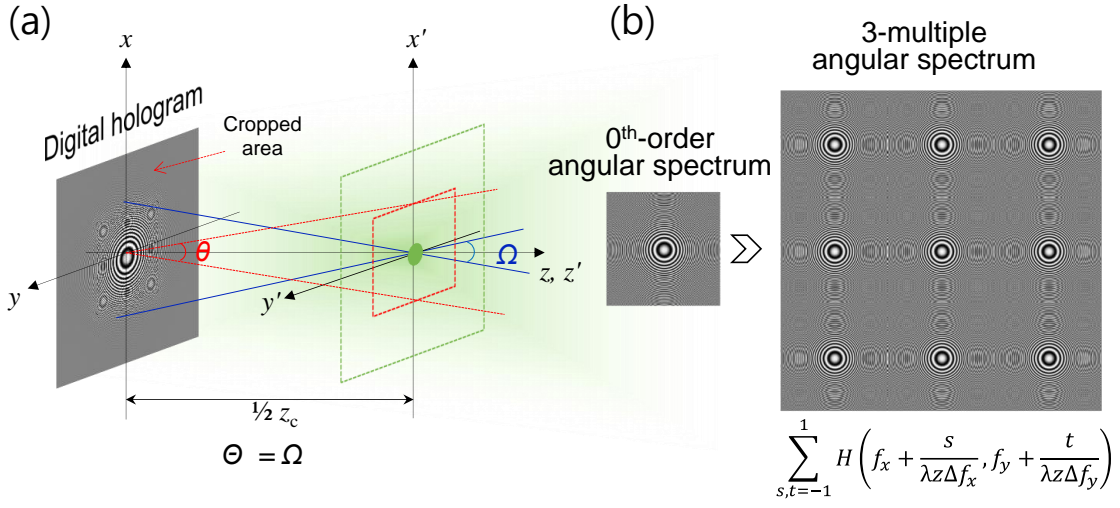


FIG. 2: (a) Digital holographic system via the convolutional method. (b) Expansion of the angular spectrum of digital hologram. The hologram for a point object is depicted for convenience.

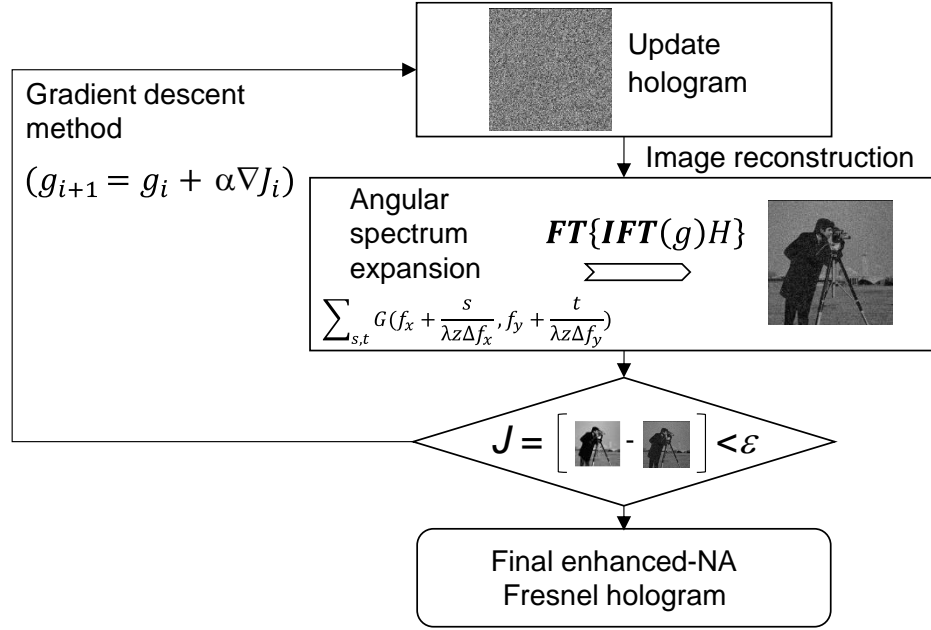


FIG. 3: Flowchart of the proposed algorithm for optimizing the enhanced-NA Fresnel hologram to recover the low space-bandwidth.

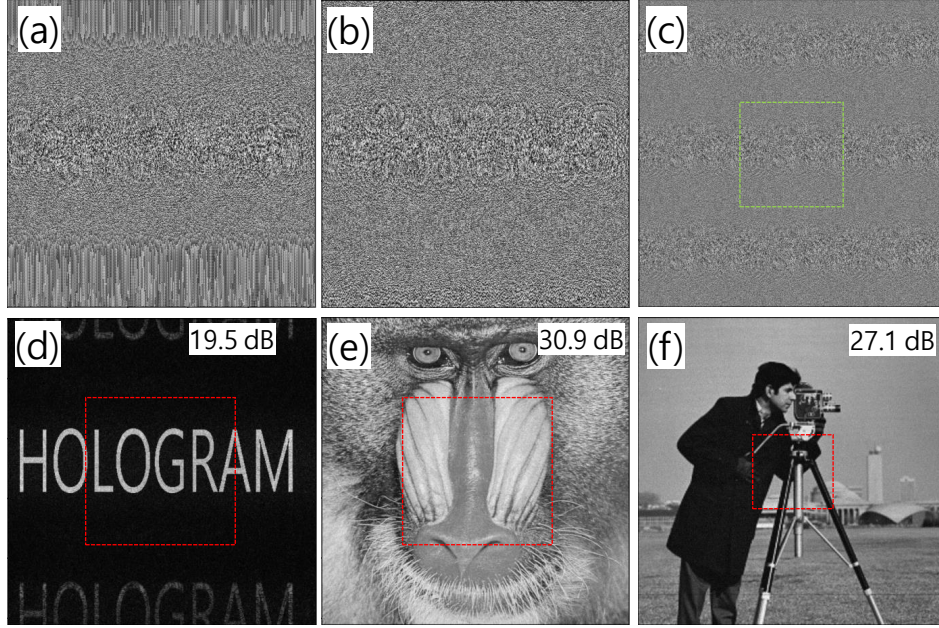


FIG. 4: Simulation results of the proposed algorithm. Digital holograms made via the processes (a) without and (b) with the angular spectrum expansion. (c) The angular spectrum in green box is placed at a repetitive interval. (d) Sparse letter image is reconstructed from the hologram synthesized at half- z_c . Reproduced dense images from the hologram made at (e) half- z_c and (f) quarter- z_c , respectively. Red boxes indicate the diffraction zone by a hologram pixel pitch.

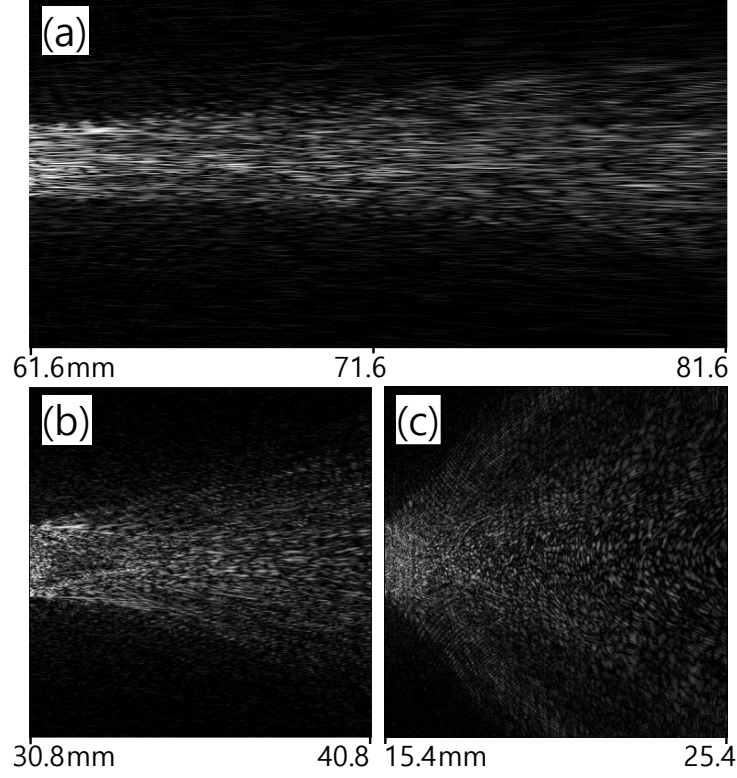


FIG. 5: Diffractive waves propagating away from the focused images. The focused images are generated from the holograms synthesized at (a) a critical distance z_c , (b) half- z_c , and (c) quarter- z_c , respectively. Lateral sizes of the corresponding images are $4096 \mu\text{m}$, $2048 \mu\text{m}$, and $1024 \mu\text{m}$, respectively.

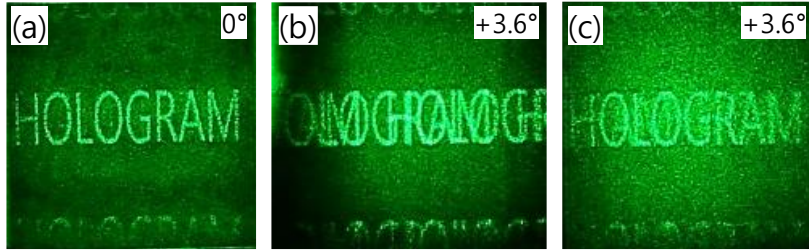


FIG. 6: (a) Optically captured images in the viewing direction of the zeroth order. Captured images in the angularly shifted direction to the first-order viewing zone (b) without and (c) with the angular spatial filter.